applied sciences

MDPI

Article

Designs of Particle-Swarm-Optimization-Based Intelligent PID Controllers and DC/DC Buck Converters for PEM Fuel-Cell-Powered Four-Wheeled Automated Guided Vehicle

Mehmet Hakan Demir [1,2,*] and Mehmet Demirok [3]

[1] Department of Mechanical and Industrial Engineering, University of Illinois at Chicago, Chicago, IL 60607, USA
[2] Department of Mechatronics Engineering, Iskenderun Technical University, 31200 Iskenderun, Hatay, Turkey
[3] Department of Mechanical Engineering, Iskenderun Technical University, 31200 Iskenderun, Hatay, Turkey
* Correspondence: mdemir4@uic.edu or mhakan.demir@iste.edu.tr

Abstract: For automatic guided vehicles (AGVs), maximizing the operating time with maximum energy efficiency is the most important factor that increases work efficiency. In this study, the fuel-cell-powered AGV (FCAGV) system was modeled and optimized control and design were carried out to obtain high tracking performance with minimum power consumption. Firstly, a full mathematical model of FCAGV, which involves the AGV, the fuel cell, DC/DC converters and motors, was obtained. Then, particle swarm optimization (PSO)-based intelligent PID and I controllers were developed for maximizing the route-tracking performance of AGV and voltage-tracking performance of the DC/DC converter with reduced power consumption. PSO was used to determine the optimal parameters of controllers and the values of DC/DC converters' components. The performance of the full AGV system was analyzed for different paths. The results show that the sufficient path-tracking and voltage-tracking performance was obtained for AGV and DC/DC converters, respectively. The average tracking errors according to global coordinate system are 0.0061 m at the x axis, 0.0572 m at the y axis and 0.0228 rad at rotational axis. The obtained average voltage-tracking errors for each DC/DC converters were approximately 0.8033 V. These results indicate that the developed controllers with optimal coefficients work successfully with small voltage and path-tracking errors. During this motion, the average consumed power from the fuel cell was observed as 58.2675 W. These results show that the designed optimized intelligent controllers have sufficient performance with high energy efficiency and maximum route tracking.

Keywords: AGV; control; design; PEMFC; optimization; PSO; power consumption; DC/DC converter

Citation: Demir, M.H.; Demirok, M. Designs of Particle-Swarm-Optimization-Based Intelligent PID Controllers and DC/DC Buck Converters for PEM Fuel-Cell-Powered Four-Wheeled Automated Guided Vehicle. *Appl. Sci.* **2023**, *13*, 2919. https://doi.org/10.3390/app13052919

Academic Editors: Bor-Ren Lin and Ke-Han Su

Received: 17 January 2023
Revised: 18 February 2023
Accepted: 22 February 2023
Published: 24 February 2023

1. Introduction

An AGV is a portable robot that follows marked lines or wires on the ground or uses radio waves, cameras, magnets or lasers for navigation. Computer-controlled and wheel-based AGVs are load carriers that travel across the floor of a facility without an onboard operator or driver. AGVs are also used to repeat transport duties in other areas such as warehouses, container terminals and external (underground) transport systems [1,2]. Studies on AGV in the literature have generally focused on AGV design, trajectory control and power consumption analysis. In the light of the information in the literature, factors such as the number of pick-up and drop-off points, route, traffic management, flow path layout, vehicle requirements and battery management are important in the design of AGV. Kaloutsakis et al. [3] worked on a low-cost AGV design in their studies and created a frame for an AGV that can carry a 200 kg load and performed its structural tests. A different design of a high-payload AGV with Mecanum wheels was created by Chen et al. [4]. For this AGV carrying at least 740 kg, engine power analysis and route-tracking performance during motion were examined. Lin [5] designed a six-wheel magnetic-navigation-based

AGV and observed successful route tracking with fast response and strong stability with its fuzzy-logic controller. There are many patents and papers in the literature for many AGVs produced for different purposes [6–10].

Another criterion that stands out regarding the performance of AGVs is the tracking performance of the given routes. AGVs can move along different routes according to the task and the environment in which the task takes place. Since they work together with other factors in an environment, it is very important for them to follow this determined route, both in terms of efficiency and security. For this reason, many studies in the literature have focused on modeling and trajectory control of AGVs. Since AGVs are a type of mobile robot, studies on modeling are generally based on mobile robots. These robot types differ according to the number of wheels and wheel designs. The kinematic and dynamic modeling of a mobile robot with four mechanical wheels was investigated by Zeidis and Zimmermann [11] and Hendzel and Rykala [12] under different conditions. Another type of four-wheeled mobile robots are robots that can be driven and rotated independently on four wheels, and their kinematic and dynamic modeling has been studied by Makatchev and McPhee [13] and Cherubini et al. [14]. Three-wheeled mobile robots are also used for AGVs. In these mobile robots, while the rear two wheels are fixed, the front wheel can have a non-holonomic structure, and there are types in which each wheel can be controlled separately. The dynamic and kinematic models of three-wheeled mobile robots have been studied in detail in the literature [15–17].

When the studies on trajectory control, which is one of the performance criteria for robots for which mathematical models are obtained, are examined, it is seen that many control techniques and approaches are used to achieve successful tracking performance. For two-wheeled AGVs, a model predictive control-based control strategy was developed by Xu et al. [18], and an improved reaching-law-based sliding mode controller was developed by Han et al. [19]. For the control of a three-wheeled AGV, Chen et al. [20] developed a sliding mode variable structure control theory based on a new control rule with the Lyapunov method. Other studies on the control of a three-wheeled AGV include a new control strategy based on the Udwadia–Kalaba approach [21], time-varying state feedback control [22], adaptive learning-based model predictive control strategy [23] and the linear parameter varying control strategy [24]. For the control of four-wheeled AGVs, many techniques have been similarly applied. These include model predictive control [25], a kinematic nonlinear controller based on Lyapunov stability [26], fuzzy reasoning [27], a backstepping-method-based controller [28] and an output-constraint control strategy (hyperbolic method) [29]. There are many studies in the literature on orbital control of AGVs. This technique can be applied to AGVs in all orbital controllers applied to mobile robots. Control and motion planning studies in this area were collected by Sánchez-Ibáñez et al. [30] and He et al. [31]. Readers can refer to these studies for more information.

AGVs have power systems that store energy and convert it into mechanical rotational or translational energy at the desired rate to enable mobile operation. These power systems include the element that provides energy and the motors that take energy from this element and convert it into mechanical energy. The use of energy is an important criterion to increase the efficiency of use of the mobile robot. The ability of robots to perform given tasks for a long time without stopping depends on the efficient use of energy in the robot. For this purpose, the selection of the energy source and the correct management of the energy are of great importance. There are studies on the energy consumption of AGVs, which are expected to work independently from the energy source as much as possible and to be able to do this for as long as possible, according to the route, the load carried and the route-tracking performance [32–35]. Batteries are generally used as an energy source in AGVs. The literature includes studies on energy management for AGVs using batteries, AGV battery life cycle management [36], AGV battery management for Industry 4.0 applications [37], analysis of battery management using system dynamics [38], energy consumption and, accordingly, the development of a charging strategy [39,40]. However, as can be seen from these studies, AGVs with batteries need frequent battery replacement

or charging according to their duties. This causes loss of time during the task and a decrease in work efficiency. For this purpose, the use of hydrogen fuel cells with higher energy density in mobile robots has increased as an energy source. Hydrogen fuel cells are an incredibly versatile technology with a wide variety of applications and are used in the material handling industry, with more than 25,000 hydrogen fuel cell forklifts used in warehouses, stores and manufacturing facilities across the USA. Fuel cells, which are highly preferred in vehicles and mobile robots due to their advantages such as energy efficiency, positive impact on the environment, low noise and size, have disadvantages such as expensive production and difficulties in the production and storage of hydrogen used as fuel. Kendall et al. [41] investigated the prolongation of the battery operating time for mobile robot by adding a microtubular SOFC generator. Guizzi et al. [42] designed a hybrid energy system for small mobile non-automotive devices, and the effects of the combination of energy system components on the energy efficiency were investigated. Lü et al. [43] studied energy and performance optimization by applying a cloud-model-based fuel cell hybrid energy system to a mobile robot used for welding, and the performance of an AGV power supply system with a polymer electrolyte membrane fuel cell stack (PEMFC) was assessed by Niestroj et al. [44] to minimize vehicle downtime. As can be seen, the number of studies on the use of hydrogen fuel cells for mobile robots has increased in recent years, while there are few studies in which fuel cells are used as an energy source in heavy load systems such as AGVs.

As can be seen from the articles reviewed, systems where alternative energy sources are used for energy come to the fore, considering the depletion of fossil fuel resources and the damage they cause to the environment. Autonomization is of great importance for both human health and work efficiency in vehicles such as AGVs and forklifts operating in closed environments such as factories. It is very critical in terms of efficiency that the tasks are carried out promptly, with reduced cost, long working performance and with few mistakes. For this reason, while autonomous vehicles such as AGVs provide route-tracking performance and high performance, minimum power consumption requirements arise. For this purpose, control algorithms that increase route-tracking performance have been developed in the studies examined, and attempts have been made to increase energy efficiency by driving different alternative energy sources with maximum power tracking algorithms. In this study, route-tracking performance and power consumption of a fuel-cell-powered AGV system with four mechanical wheels were investigated with PSO-based PID controllers. The studies in the literature have been extended with the development of PSO-based controllers to provide maximum performance route tracking of a fuel-cell-powered four-wheeled AGV with minimum power consumption. In addition, R, L and C values for DC/DC converters were determined by PSO-based optimization in order to obtain maximum voltage-tracking performance and minimum power consumption. The contributions of this paper are as follows:

- The full FCAGV system was modeled by combining the mathematical models of a four-Mecanum-wheeled AGV, a PEM fuel cell system, DC/DC buck converters and the motors of the AGV.
- A PSO-based PID controller was developed to obtain maximum route-tracking performance of AGV with reduced power consumption (Optimizer-1).
- A PSO-based I controller was developed to obtain maximum voltage-tracking performance with reduced power consumption for DC/DC converters (Optimizer-2).
- The values of resistance, inductance and capacitance of DC/DC converters were optimized by using the PSO algorithm for voltage-tracking/power-consumption optimization (Optimizer-2).

Hendzel and Rykala's model in [12], which is one of the most comprehensive four-wheeled AGV models in the literature, was used and extended in this study by adding mathematical models of the DC motor, DC/DC buck converter and PEM fuel cell. In order to perform analysis including all system equipment, a model of the whole system was created. With the help of this model, the voltage and power required to be fed

by the fuel cell were determined in order for the AGV to have the desired positions in the x and y axes and the rotation around the z axis according to the general coordinate system. During the movement, each motor is controlled separately, and their overall power requirement changes throughout the movement. In order to achieve maximum route-tracking performance with minimum power consumption, the coefficients of PID controls designed for each engine and both integral (I) control coefficients and resistance, capacitor and coil values of DC/DC converters, which ensure that the consumed power from the fuel cell is reduced to the desired level before reaching the engines, were obtained using the PSO algorithm. System parameters such as power consumption, route-tracking performance, the power consumed by the engines and the hydrogen and air supply of the fuel cell were examined for the different routes determined by the simulations made in line with the obtained values. The results show that the designed optimized intelligent controllers and DC/DC converters have sufficient voltage/route-tracking performance with reduced power consumption.

The mathematical models of each part of the full FCAGV system are described in Section 2. In Section 3, the developed PSO-based PID and I control strategies are considered, and the algorithms of PSO-based optimizers are described in this section. The optimized parameters for controllers and the obtained performance results for different paths test are given in Section 4. Finally, the key results, importance of these results and future work are outlined in Section 5.

2. System Modeling

This study utilized a general AGV system, mechanical four-wheeled mobile robot, DC motors, DC/DC buck converters and fuel cell. The system block diagram is shown in Figure 1. The inputs and the outputs of all subsystems are clearly shown in Figure 1. It shows that voltage and current are supplied by the PEM fuel cell (V_{cell} and i_{cell}, respectively). With the power fed from the fuel cell, the necessary voltages and currents of motors, which are determined by the Optimizer-1-optimized PID controller, are sent to the motors of the mecanum wheels. However, the voltage value at the fuel cell output is a high value for the engines operating in the $\pm$24 V range that we use in the system. For this reason, it needs to be lowered with the help of the DC/DC converter. However, the voltage value required by each motor throughout the motion varies depending on its speed. Wheel speeds are changed during the course with the PID controller, which is designed for full tracking of the route, and accordingly, the voltage value required by the motors changes in the range of $\pm$24 volts. For this reason, DC/DC converters need to adjust the voltage value from the fuel cell as needed by the engine. For this purpose, an integral (I) controller was designed for each DC/DC converter. After the necessary inputs for the motors are tracked successfully by the DC/DC converters, the output signals of the converters are sent to motors. These voltage inputs generate rotational motions and torques of the motors. Then, the speeds of the motors and torque values are used in the dynamics of the AGV system, and the actual position and rotation of the mobile robot are determined. After that, these actual and reference values of the mobile robot are compared and are evaluated in Optimizer-1, and the optimal PID parameters are obtained to track the reference route with minimum errors. Then, the calculated control inputs for the motors are sent to the DC/DC converters as reference voltages for tracking. Optimizer-2 tries to minimize the power consumption and voltage-tracking errors at the output of the converters by comparing the determined control inputs for motors and actual output voltages of converters. By using these data, Optimizer-2 determines the values of the resistor, inductance and capacitance of each converter and I coefficient of the controller in the converters. The coefficients of both PID and I controllers and the components of the DC/DC converters were determined on the basis of maximum route tracking and minimum power consumption with the PSO technique. By providing the desired voltage at the DC/DC converter output, the motors rotate at the desired speed, and the route tracking is successfully achieved.

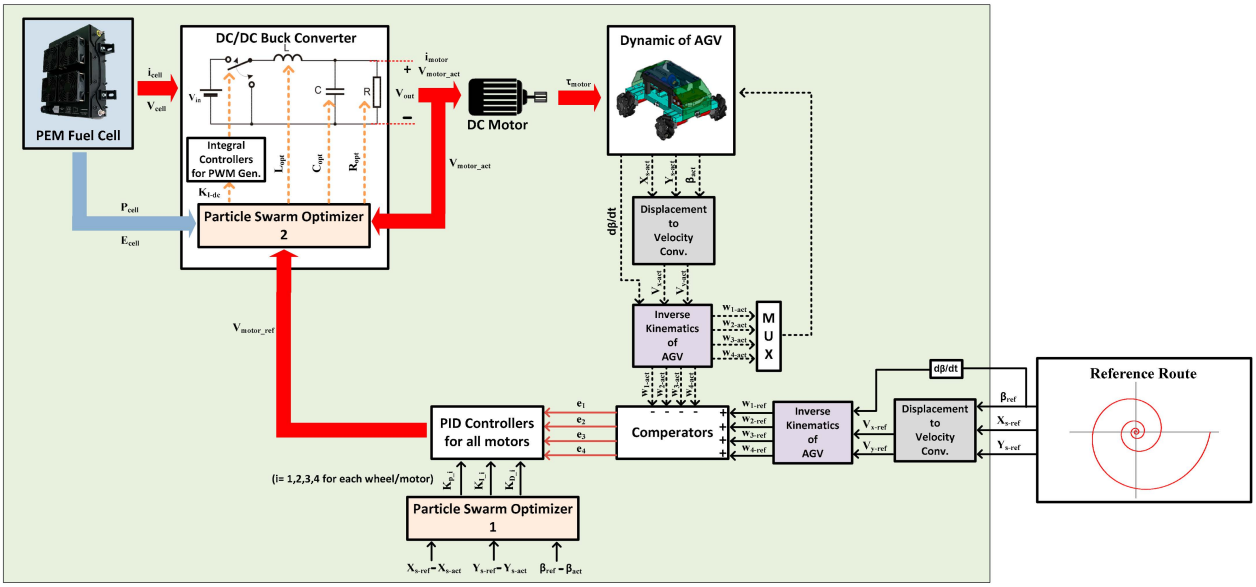

Figure 1. The schematic diagram of the four-Mecanum-wheeled AGV system.

2.1. Four-Wheeled Mobile Robot Modeling

In this study, the model obtained by Hendzel and Rykala [12], one of the most comprehensive models in the literature, was used as the kinematic and dynamic model of the mobile robot part of the AGV system, which was designed with four mechanical wheels. A two-dimensional coordinate system representation of AGV is shown in Figure 2.

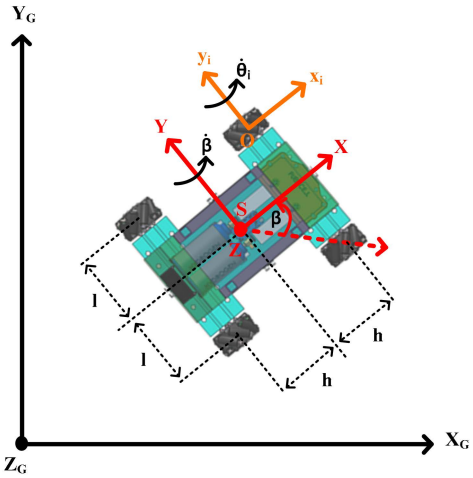

Figure 2. Two-dimensional coordinate system representation of AGV.

Using this schematic diagram of the AGV with four Mecanum wheels, the kinematic and dynamic models were obtained by using Lagrange energy method, and the kinematic model and inverse kinematic model of this AGV are given in Equations (1)–(7). Firstly, the angular velocities of the wheels were obtained with inverse kinematics equations by using the linear velocities and angular rotation during the motion of the AGV.

Inverse kinematic model:

$$\dot{\theta_1} = \frac{1}{(R+r)}\left(V_x - V_y - \dot{\beta}(h+l)\right) \quad (1)$$

$$\dot{\theta_2} = \frac{1}{(R+r)}\left(V_x + V_y + \dot{\beta}(h+l)\right) \quad (2)$$

$$\dot{\theta_3} = \frac{1}{(R+r)}\left(V_x + V_y - \dot{\beta}(h+l)\right) \tag{3}$$

$$\dot{\theta_4} = \frac{1}{(R+r)}\left(V_x - V_y + \dot{\beta}(h+l)\right) \tag{4}$$

where R, r, h and l denote the mechanical properties of the AGV, specifically the radius of the Mecanum wheel's cylinder, the radius of the wheel, the horizontal (x direction) distance between the vehicle's midpoint and a wheel and the vertical (y direction) distance between the vehicle's midpoint and a wheel, respectively. θ_i and $\dot{\theta_i}(i = 1, 2, 3, 4)$ indicate the angular velocities of each Mecanum wheel, and $V_j(j = x, y)$ and $\dot{\beta}$ are the linear velocities and angular velocity of the AGV according to the local coordinate system at the center of the AGV.

Vice versa, the kinematic equations of the system were used if the linear velocities and angular velocity of the AGV were required depending on the angular velocities of the AGV's wheels.

Kinematic model:

$$V_x = \left(\frac{R+r}{4}\right)\left[\dot{\theta}_1 + \dot{\theta}_2 + \dot{\theta}_3 + \dot{\theta}_4\right] \tag{5}$$

$$V_y = \left(\frac{R+r}{4}\right)\left[-\dot{\theta}_1 + \dot{\theta}_2 + \dot{\theta}_3 - \dot{\theta}_4\right] \tag{6}$$

$$\dot{\beta} = \left(\frac{R+r}{4(h+l)}\right)\left[-\dot{\theta}_1 + \dot{\theta}_2 - \dot{\theta}_3 + \dot{\theta}_4\right] \tag{7}$$

The linear velocities and angular velocity were also found by using the relationship between the velocities and rotation according to the global coordinate system. These relationships have to be used to determine the necessary values of the angular velocities of the wheels depending on the given route of the AGV. The equations, which define these relationships between the global and local coordinates and present the method of converting the global route to local variables, are given below.

$$V_x = \dot{x}_s \cos\beta + \dot{y}_s \sin\beta \tag{8}$$

$$V_y = -\dot{x}_s \sin\beta + \dot{y}_s \cos\beta \tag{9}$$

After this stage, the dynamic equations, in which the forces and torques acting on the system are taken into account and the linear motion of the robot is analyzed against the motor torques throughout the motion, were obtained by using the Lagrange energy method.

$$\left(m_c + \frac{4I_k}{(R+r)^2}\right)\left[\cos\beta\left(\ddot{x}_s + \dot{y}_s\dot{\beta}\right) + \sin\beta\left(\ddot{y}_s - \dot{x}_s\dot{\beta}\right)\right] = \left(\frac{1}{R+r}\right)\left[\tau_1 + \tau_2 + \tau_3 + \tau_4 - \frac{G_r f}{4}\left(\mathrm{sgn}\dot{\theta}_1 + \mathrm{sgn}\dot{\theta}_2 + \mathrm{sgn}\dot{\theta}_3 + \mathrm{sgn}\dot{\theta}_4\right)\right] \tag{10}$$

$$\left(m_c + \frac{4I_k}{(R+r)^2}\right)\left[\cos\beta\left(\ddot{y}_s - \dot{x}_s\dot{\beta}\right) - \sin\beta\left(\ddot{x}_s + \dot{y}_s\dot{\beta}\right)\right] = \left(\frac{-1}{R+r}\right)\left[\tau_1 - \tau_2 - \tau_3 + \tau_4 - \frac{G_r f}{4}\left(\mathrm{sgn}\dot{\theta}_1 - \mathrm{sgn}\dot{\theta}_2 - \mathrm{sgn}\dot{\theta}_3 + \mathrm{sgn}\dot{\theta}_4\right)\right] \tag{11}$$

$$(I_c + 4I_k)\frac{(a+b)^2}{(R+r)^2}\ddot{\beta} = \frac{-(a+b)}{(R+r)}\left[\tau_1 - \tau_2 + \tau_3 - \tau_4 - \frac{G_r f}{4}\left(\mathrm{sgn}\dot{\theta}_1 - \mathrm{sgn}\dot{\theta}_2 + \mathrm{sgn}\dot{\theta}_3 - \mathrm{sgn}\dot{\theta}_4\right)\right] \tag{12}$$

As can be seen from the dynamic model equations, when the obtained differential equations are solved, the linear parameters of the mobile robot (linear positions, velocities and acceleration in the x and y directions and angular position, velocity and acceleration) are calculated depending on the torque values applied by the motors. In system dynamics where internal and external forces acting on the system are taken into account, τ_i is the driving torque originating from the power transmission system. $m_c(m_c = m_A + 4m_T)$, I_k, $I_c(I_c = I_A + 4I_T)$, $G_r(G_r = G_A + 4G_T)$ and f represent total mass of the robot, the moment of inertia of the wheels on their own axis, the total moment of inertia of the system on the z axis and the total weight of the system and coefficient of rolling friction for each wheel (equal for all wheels), respectively. m_A is the mass of the chassis of the robot and m_T is the

mass of each wheel. Similarly, G_A is the weight of the chassis of the robot and G_T is the weight of each wheel. I_A and I_T denote the moment of inertia of the mobile robot base and each wheel on the z axis, respectively. The parameters for the AGV which were used for the simulations in this study are given in Table 1.

Table 1. The values of the AGV's parameters.

Parameter	Value (Unit)	Parameter	Value (Unit)
Mass of load on AGV (M_t)	45 (kg)	Radius of wheel (R)	0.055 (m)
Mass of AGV (M_p)	10 (kg)	Radius of cylinder (r)	0.015 (m)
Mass of wheel (M_k)	1.5 (kg)	Distance in y axis (l)	0.49 (m)
Total mass (M_{pc})	$M_p + 4M_k + M_t$ (kg)	Distance in x axis (h)	0.46 (m)
Moment of inertia of AGV ($I_{p_{zp}}$)	0.0178 (kg·m^2)	Coefficient of friction (f)	0.002 (kg·m/s)
Moment of inertia of wheel ($I_{k_{zp}}$)	0.0139 (kg·m^2)	Total AGV weight (G_r)	9.81M_{pc} (N)
Total moment of inertia (I_{pc})	$I_{p_{zp}} + 4I_{k_{zp}}$ (kg·m^2)	Reaction forces (N_i)	$G_r/4$ (N)
Axial inertia of each wheel (I_k)	0.0005 (kg.m^2)	Radius of cylinder (r)	0.015 (m)

After that, this model of AGV was combined with the models of the other system components. Figure 1 shows the relationship between these components and their models, and it can be seen that the torques of the motors and rotational velocities of the wheels are needed to calculate to obtain the linear displacements and rotation according to global coordinates.

2.2. DC Motor Model

A classical brushless direct current motor was used for propulsion on each wheel of the AGV, and the motor model equations were obtained by using the free body diagram of this DC motor. In Figure 3, the schematic representation of the classical DC motor is given. In this figure, V_{motor}, I_{motor}, R_i, L_i, E_i and τ_i denote voltage of the ith motor, current of the ith motor, electrical resistance and inductance of the motor, electromotor voltage and torque of the ith motor, respectively.

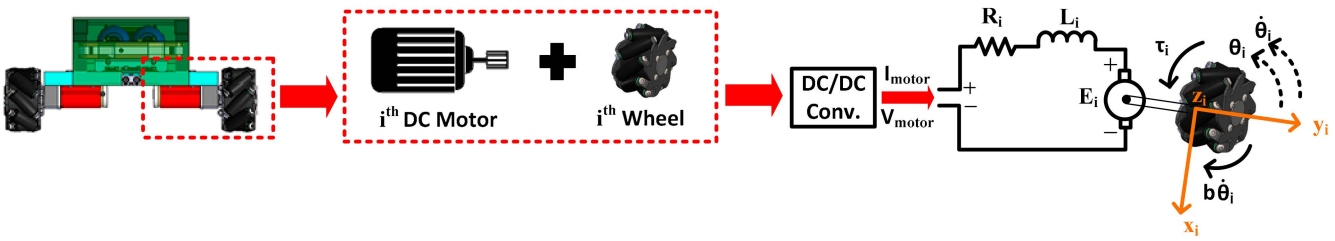

Figure 3. Schematic diagram of ith DC motor.

According to this diagram, the transfer function that gives the connection between the motor supply voltage and the motor rotational speed is given below [45].

$$\frac{\dot{\theta}_i(s)}{V_{motor}(s)} = \frac{K_i}{(Js+b)(L_i s + R_i) + K_i^2} \left[\frac{rad/\,sec}{V}\right] \tag{13}$$

where J, K_i, ($K_i = K_e = K_t$) and b denote the moment of inertia of the rotor, the motor constant and motor' viscous friction constant. The used values of each DC motor's parameters are given in Table 2. Using Equation (13), the voltage from DC/DC converters was converted to wheel angular velocities for use in dynamic and inverse kinematic models of AGV.

Table 2. The values of the DC motor's parameters.

Parameter	Value (Unit)
Motor viscous friction (b)	0.250 (kg·m^2/s)
Motor constant ($\mathbf{K_i}$)	0.002 (Nm/A)
Moment of inertia of the rotor (J)	0.15 (kg·m^2)
Inductance ($\mathbf{L_i}$)	0.12 (H)
Resistance ($\mathbf{R_i}$)	0.5 (Ω)

2.3. DC/DC Buck Converter Model

The DC/DC buck converter reduces the voltage (input voltage, V_s) value it receives from the hydrogen fuel cell to the required voltage (output voltage) value for the motor with the help of an integral (I) controller. The output voltage V_0 is calculated according to the current and voltage value passing over the inductor when the switch in the converter circuit is open or closed. The comparison of the time between the switch on and off is carried out with the duty cycle (DT). By setting the DT between 0 and 1, the on and off times of the switch are adjusted. Depending on this value, the output voltage is obtained using the following equations, depending on the input voltage of the system [46,47].

$$(\Delta i_L)_{CLOSED} = \left(\frac{V_S - V_0}{L}\right) DT \tag{14}$$

$$(\Delta i_L)_{OPEN} = -\left(\frac{V_0}{L}\right)(1 - DT) \tag{15}$$

$$(\Delta i_L)_{CLOSED} + (\Delta i_L)_{OPEN} = 0 \tag{16}$$

The DC/DC buck converter internal structure consisting of an RLC circuit, and the MOSFET creates the output voltage over the resistor inside by controlling the PWM signal that triggers the MOSFET switching by an integral controller. A positive voltage value from the fuel cell is constantly received by the DC/DC converter input. However, while the AGV follows the determined route, the direction of rotation of the motors changes, and accordingly it is necessary to send positive and negative voltages to the motors. In cases where the positive high voltage at the output of the fuel cell is required, depending on the voltage needed to turn it into negative, the voltage value at the DC/DC converter output is inverted, and its negative value can be obtained. A diagram of the obtained DC/DC converter system is given in detail in Figure 4.

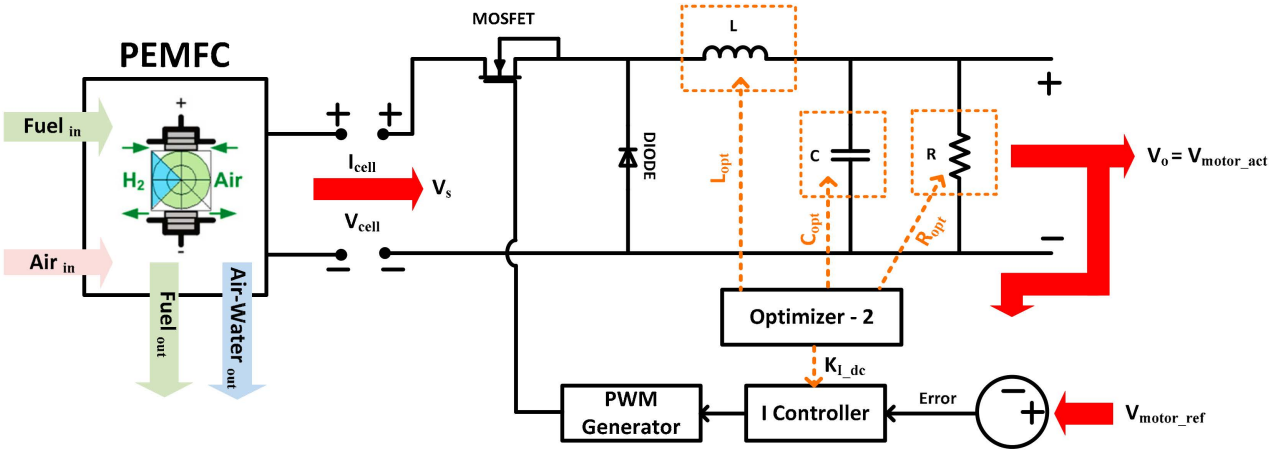

Figure 4. Block diagram of DC/DC buck converter jth (j = 1, 2, 3, 4).

In addition, 10,000 Hz was determined as the switching frequency (f_s) for the DC/DC converter. In line with the information in the literature, this value is good for a low-power system.

2.4. Fuel Cell Model

For the PEM fuel cell (PEMFC) model, the fuel cell model in the MATLAB/Simulink library was used [48]. The block diagram created for the PEM fuel cell, the output of which is directly given to the DC/DC converters, is shown in Figure 4, and the characteristics of the fuel cell are given in Table 3.

Table 3. Specification of PEMFC [48].

Property	Value
Model	24 V DC PEMFC
Nominal and maximum power	1.26 KW–2 KW
Voltage at 0A and 1A	V(0A) = 42 V, V(1A) = 35 V
Nominal working point	I_{nom} = 52 A, V_{nom} = 24.23 V
Max. operation point	I_{end} = 100 A, V_{nom} = 20 V
Cell number	42
Stack efficiency	46%
Working temperature	55 °C
Nominal air outlet rate	2400 lpm
Nominal supply pressure	Fuel: 1.5 bar, air: 1 bar
Nominal composition	99.95% H_2, 2% O_2, 1% H_2O

As seen in the figure, voltage, current, stack energy and fuel consumed by the stacks and air data are collected at the fuel cell output. By evaluating these data, the power consumed by the fuel cell was analyzed and used in the optimization study to increase energy efficiency.

After the modeling process of all system components was completed and their relationships with each other were defined, a wide model was obtained in which linear and angular displacements are obtained from the fuel cell output voltage according to the global coordinate system of the AGV, as stated above. By using this model, the control strategy design, in which the parameters of the controllers and DC/DC converter parameters are optimized, was carried out in order for the system to achieve maximum route-tracking performance with the least power consumption.

3. Control Strategy

Optimally adjusting the controller parameters improves system performance and ensures a successful response in changing system conditions. While various methods are used to adjust the controller parameters, they can be grouped as theoretical, experimental and with the help of artificial intelligence. While the controller parameters can be calculated with theoretical methods using the data obtained at the output of the system, this situation may not provide the appropriate control success in case of situations such as the system being under external influence. When finding these parameters experimentally, while successful results can be produced, the time spent can be high, and there is absolutely no guarantee that good results can be achieved. Utilizing artificial-intelligence methods is another method of overcoming these problems. There is no guarantee that the optimum solution will be found with the use of these techniques, but the time taken to find the ideal parameters for the expected result in the system output is reduced. In this study, an optimized PID controller was designed for route-tracking control of the FCAGV and I controller for voltage-tracking control of DC/DC converters. While PID controllers can be easily applied in linear systems and systems with a stable progress, it is important to determine the parameters correctly in order to give successful results in the control of uncertain, time-varying, complex and nonlinear systems [49,50]. In such cases, when artificial-intelligence techniques are not used, it becomes time-consuming and difficult to reach optimum values. Combining the PID method with other artificial-intelligence methods to create more efficient control systems gives successful and sufficient results in the control of many systems. The PID controller combined with the optimization theories

such as particle swarm optimization (PSO) [51], genetic algorithms (GAs) [52] gray wolf optimization (GWO) [53] and artificial bee colonies (ABCs) [54] can facilitate a more flexible, robust and improved control performance. For this reason, the parameters of controllers and DC/DC converters were adjusted according to process conditions using the PSO algorithm in this study to increase the route/voltage-tracking performance and power consumption efficiency.

3.1. Particle Swarm Optimization (PSO)

The particle swarm optimization (PSO) method has been widely used for many years. The PSO algorithm, first developed by Kennedy and Eberhart in 1995, was inspired by the social behavior of flying flocks [55].

While the PSO algorithm sets the PID parameters in this study, it starts with a random position of all particles in the search space, and the positions of the particles are updated according to two values at each step. The first is the previous best solution, called p_{best}. The other is the best result from all iterations since the first iteration, and this result is the optimum PID parameter value found. It is called global best or g_{best}. The search continues in the PSO until the specified number of iterations is reached or the optimum error value is reached. The swarms of particles progressively continue until the specified number of iterations is reached, constantly updating speed and position information to be optimal. The position update formula for the particles used in this study is:

$$\begin{aligned} V(k+1) = w(k+1)\,V(k) + c_1(k+1)\,rand_1\,(P^{lbest}(k+1) - P(k)) \\ +c_2(k+1)\,rand_2\,(P^{gbest}(k+1) - P(k)) \end{aligned} \quad (17)$$

$$P(k+1) = P(k) + V(k+1) \quad (18)$$

where V(k) denotes particle velocity and P(k) represents the particle positions. w, c_p (p = 1, 2), P^{lbest} and P^{gbest} denote the inertia weight, positive learning coefficients and the local and global best results, respectively. $rand_1$ and $rand_2$ are random numbers between 0 and 1.

Inertia weight in Equation (17) represents the momentum degree of particles. For early iterations, this value can be set higher, allowing the particles to widely explore and aggressively investigate the solution area. In order to further optimize the algorithm, this setting is gradually converted, making it smaller in later iterations, and better results can be achieved. In this study, the moment of inertia w, starting from the first iterations (w_{max}), was gradually decreased linearly to the last iterations (w_{min}). For this case, the w(k + 1) value was obtained by the following equation.

$$w(k+1) = w_{max} - \frac{w_{max} - w_{min}}{i_{max}} i \quad (19)$$

where i and i_{max} indicate the iteration's number and its maximum number, respectively. The optimization parameters used for PSO algorithms are shown in Table 4.

Table 4. The parameters of PSO algorithms for both optimizers.

	Optimizer-1	**Optimizer-2**
Number of variables	12	16
Population	20	20
Max. iteration	20	20
Wmax (inertia momentum)	20	20
Wmin (inertia momentum)	0.9	0.9
C_i (positive learning coefficients)	0.2	0.2

3.1.1. PSO-Based Optimizer-1

In this study, PSO-based optimization was used for two purposes. The first of these was to optimize the K_p, K_i and K_d values of the PID controllers for each motor to control the route-tracking performance of the AGV. The block diagram of the algorithm created for this purpose is given in Figure 5a. In this optimizer, 12 parameters are adjusted depending on the error between the reference and actual translational and rotational motions. As can be seen in the figure, the PSO algorithm determines the PID controller parameters for each motor that provide the best performance by optimizing in line with the determined initial conditions and the objective function, and the control input is created in line with the incoming error. Then, the determined optimal values for PID coefficients are used to adjust to AGV motion by using the relationship between the angular velocities of the wheels and control input voltage of the motors. The procedure of the PSO algorithm for finding best values of controllers' coefficients to obtain best tracking performance is shown in Figure 5b.

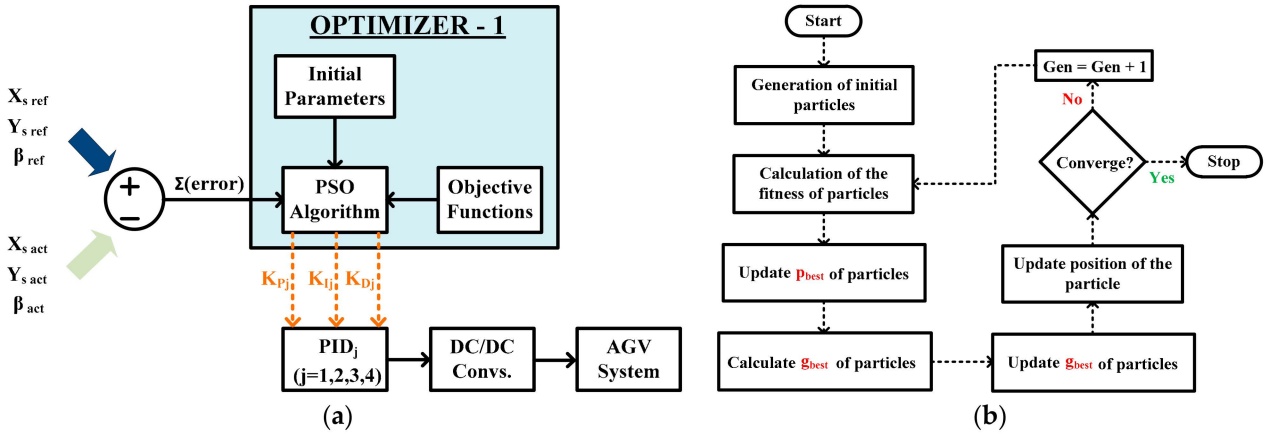

Figure 5. (**a**) PSO-based PID tuning diagram of the AGV's route-tracking control structure. (**b**) The optimization algorithm of the PSO method.

The limit values of the optimized parameters are defined in the PSO algorithm, and the optimizers try to find the optimal values of parameters for reaching the goals in these ranges. For Optimizer-1, the limits of PID controllers' parameters K_{Pj}, K_{Ij} and K_{Dj} (j = 1, 2, 3, 4) are given in Table 5.

Table 5. The limits values of PID controllers' parameters for Optimizer -1.

j = 1, 2, 3, 4	K_{P_j}	K_{I_j}	K_{D_j}
Maximum limit	7500	5000	25
Minimum limit	1	1	1

3.1.2. PSO-Based Optimizer-2

The other optimizer is used to determine the K_i value of the I controller, which controls the PWM generator inside the DC/DC buck converter, which reduces the voltage value at the output of the fuel cell to the voltage values needed for the motors, and the R, L and C values of the same converter. Optimizer-2 uses reference values of motor voltage, output voltages at the output of the DC/DC buck converters and the consumed power from the fuel cell for excitations of all motors according to control inputs, which are sent by Optimizer-1-optimized PID controllers. Optimizer-2 tries to find the best (optimal) values for the electronic components of DC/DC converters and $K_{I_{dc}}$ values for controllers of four converters' PWM generation unit to adjust the switching factor by minimizing the errors between the reference and actual output voltages and consuming power from the fuel cell. The PSO-based DC/DC converters' tuning block diagram of Optimizer-2 is shown in Figure 6.

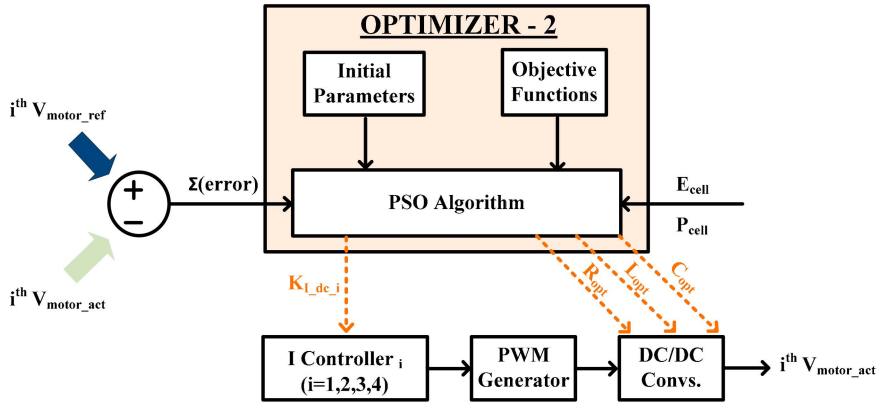

Figure 6. PSO-based integral (I) controllers' tuning block diagram of DC/DC converter optimization.

Similarly, the limits of the components' coefficients and integral coefficients of the I controllers need to be defined for the optimization procedure. For Optimizer-2, the limits of these optimized parameters are defined as shown in Table 6.

Table 6. The limits values of parameters of integral controllers and DC/DC converters' components for Optimizer -2.

(i = 1, 2, 3, 4)	$K_{I_{dc_i}}$	L_i (H)	C_i (F)	R_i (Ω)
Maximum limit	50	100×10^{-6}	1000×10^{-6}	**100**
Minimum limit	0	1×10^{-6}	1×10^{-6}	**1**

For both optimizers, the integral of time absolute error (ITAE) was chosen as the objective function for both power consumption and route-tracking optimization algorithms. The most ideal values were determined by minimizing the consumed power and the errors for the deviation in the route. The theoretical expression of the ITAE function is given in the equation below.

$$\mathrm{ITAE} = \int_0^\infty t|e(t)|dt \tag{20}$$

$$e(t) = \sum RV_i - AV_i \tag{21}$$

where RV and AV denote the reference values and actual values of the parameters, respectively. For the route-tracking process, the total error is calculated by summation of the errors of the translational and rotation motions. Similarly, the voltage-tracking errors of each converter and total power consumption of the fuel cell are used in an attempt to minimize Optimizer-2, while the PSO algorithms try to eliminate or minimize the total error for both optimizers. The optimal values of the coefficients of controllers and converters are thus determined.

4. Results and Discussion

In this study, the PSO-based optimizers were designed for adjusting the parameters of the PID controllers to improve the route-tracking performance of the AGV and adjusting the parameters of the DC/DC converters to consume minimum power from the fuel cell while increasing the route-tracking performance. The studies carried out in this study were carried out in a simulation environment using the MATLAB/Simulink program licensed by the University of Illinois at Chicago (UIC). Tests were carried out for different reference routes by combining AGV, DC/DC converters, motors and fuel cell models created in the simulation environment. The purpose of this stage was to optimize controllers and converters in terms of performance by determining the optimal parameters. Then, a different reference route was applied to the combined model with the best performance,

and route tracking, power consumption, converter voltage-tracking and fuel-consumption performance were analyzed.

As mentioned, Optimizer-1 uses the AGV's actual and reference positions for minimizing the route-tracking errors with the optimal parameters of four PID controllers, and Optimizer-2 uses the actual motor voltages (output voltage of the DC/DC converters); reference motor voltages, which are generated by the PID controllers; and the power consumption from the fuel cell. In order to determine these optimal parameters, a reference trajectory was applied to the system. Optimal values obtained as a result of this reference trajectory were also tested on another reference trajectory, and the most suitable optimal values were sought for different situations. The reference trajectory applied to determine the optimal values in the first stage is shown in Figure 7a. As can be seen in the figure, the trajectory to be followed for parameter optimization was chosen as a combination of both rotational and translational movements. The main reason for this was to determine the optimal parameters that ensure both movements of the AGV successfully and reduce power consumption while performing path tracking.

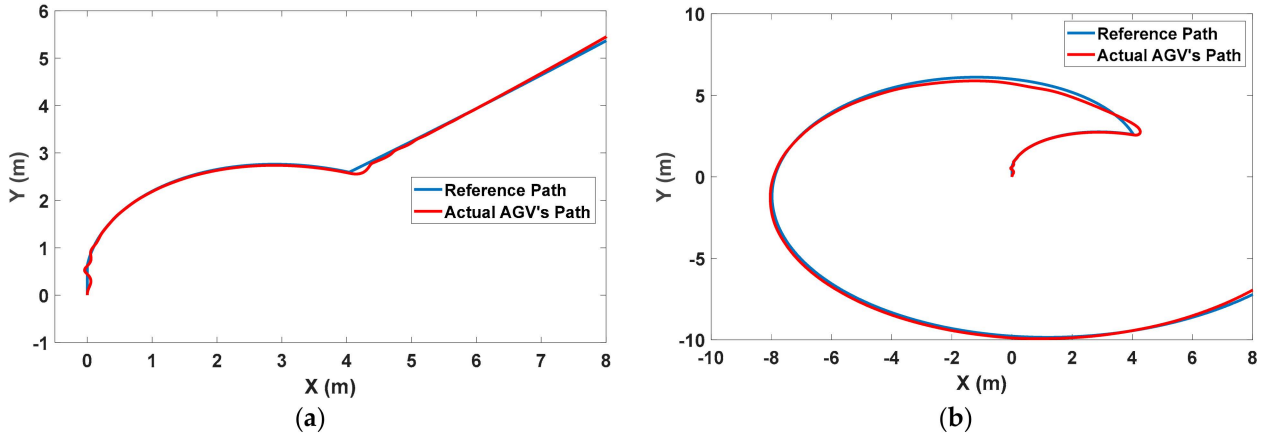

Figure 7. (**a**) The reference path for determining the optimal parameters and tracking performance with these parameters. (**b**) Testing the tracking performance of the same parameters with another path.

The optimal values calculated with this trajectory are shown in Tables 7 and 8. Table 7 shows 12 PID controller parameters determined by Optimizer-1 to follow this reference trajectory with minimum tracking error and minimum power consumption.

Table 7. The values of PID controllers' parameters optimized by Optimizer -1.

K_{P_1}	K_{I_1}	K_{D_1}	K_{P_2}	K_{I_2}	K_{D_2}
667.91830	3043.41076	6.99876	1907.50583	3154.132757	16.63205
K_{P_3}	K_{I_3}	K_{D_3}	K_{P_4}	K_{I_4}	K_{D_4}
7500	1	25	3498.62756	5000	8.10674

Table 8. The values of optimized parameters of the I controllers and DC/DC converters by Optimizer-2.

Converter	$K_{I_{dc_i}}$	L_i (H)	C_i (F)	R_i (Ω)
First motor (i = 1)	30.646195458	$2.5144095579 \times 10^{-5}$	$1.9095902447 \times 10^{-5}$	59.639317735
Second motor (i = 2)	22.747017789	$4.9990133202 \times 10^{-5}$	$6.6347926426 \times 10^{-6}$	95.972231156
Third motor (i = 3)	36.411406444	$2.4350565864 \times 10^{-5}$	$3.1518011115 \times 10^{-6}$	80.998134743
Fourth motor (i = 4)	44.0617226666	$8.2933376471 \times 10^{-5}$	$6.2723523176 \times 10^{-6}$	95.372351267

Similarly, the optimal parameters of the converters, which are determined by Optimizer-2, are given in Table 8. At this stage, four parameters are optimized for each DC/DC buck converter. The inductance, capacitance and resistance values and integral value of each converter were optimized in line with the objectives of voltage control with minimum error and keeping the energy drawn from the fuel cell as low as possible.

When the tracking performance obtained with these optimal values is examined, it is seen that a very successful trajectory tracking performance is obtained according to the results in Figure 7a. It is observed that the AGV moves with a very low error for both translational and rotational motion. In order to evaluate this successful effect of these determined parameters on trajectory tracking performance for different trajectories, the reference trajectory in Figure 7b was applied to the AGV. As can be seen, the trajectory tracking performance of the AGV has little error for this route, which includes more sharp turns than the trajectory for which the optimal parameters are determined. Thus, it can be concluded that the determined controller and DC/DC converter parameters cause successful tracking performance and can be reliably used in performance and power consumption analysis for another reference route.

After that, the spiral path was applied to the designed AGV system, and the tracking performance of the AGV is shown in Figure 8. The results show that the vehicle has sufficient and successful path-tracking performance for this route. In this route, the AGV performed both the rotational motion at different angles and the linear propagation motion in both the x and y directions with little error. This shows that the electronic design and control strategies developed for an application with this route, as in the previous routes, yield successful results. In order to better analyze the effect of optimally determined parameters on the route-tracking performance, the errors of the instantaneous x, y and beta values during the movement can also be examined relative to the reference trajectory. Figure 9 shows the time variation of the x- and y-directed displacement and velocity errors and rotation error during this motion. As can be seen from the results, the movement was completed with a small error in both translational and rotational terms. This can be considered as successful and sufficient for the AGV system used in the industry and moving between two targets. When the x and y direction translation errors along the motion shown in Figure 9a are examined, it can be seen that there is an average error of 0.0061 m in the x direction and 0.0572 m in the y direction along the entire spiral route. It can be observed from the figure that the error in the x direction is around 0.09 m maximum, and the error in the y direction is around 0.15 m maximum.

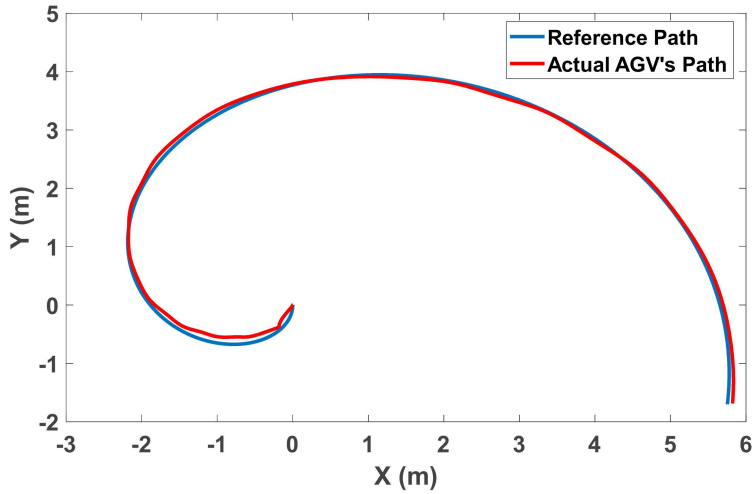

Figure 8. The path-tracking performance of AGV for spiral path.

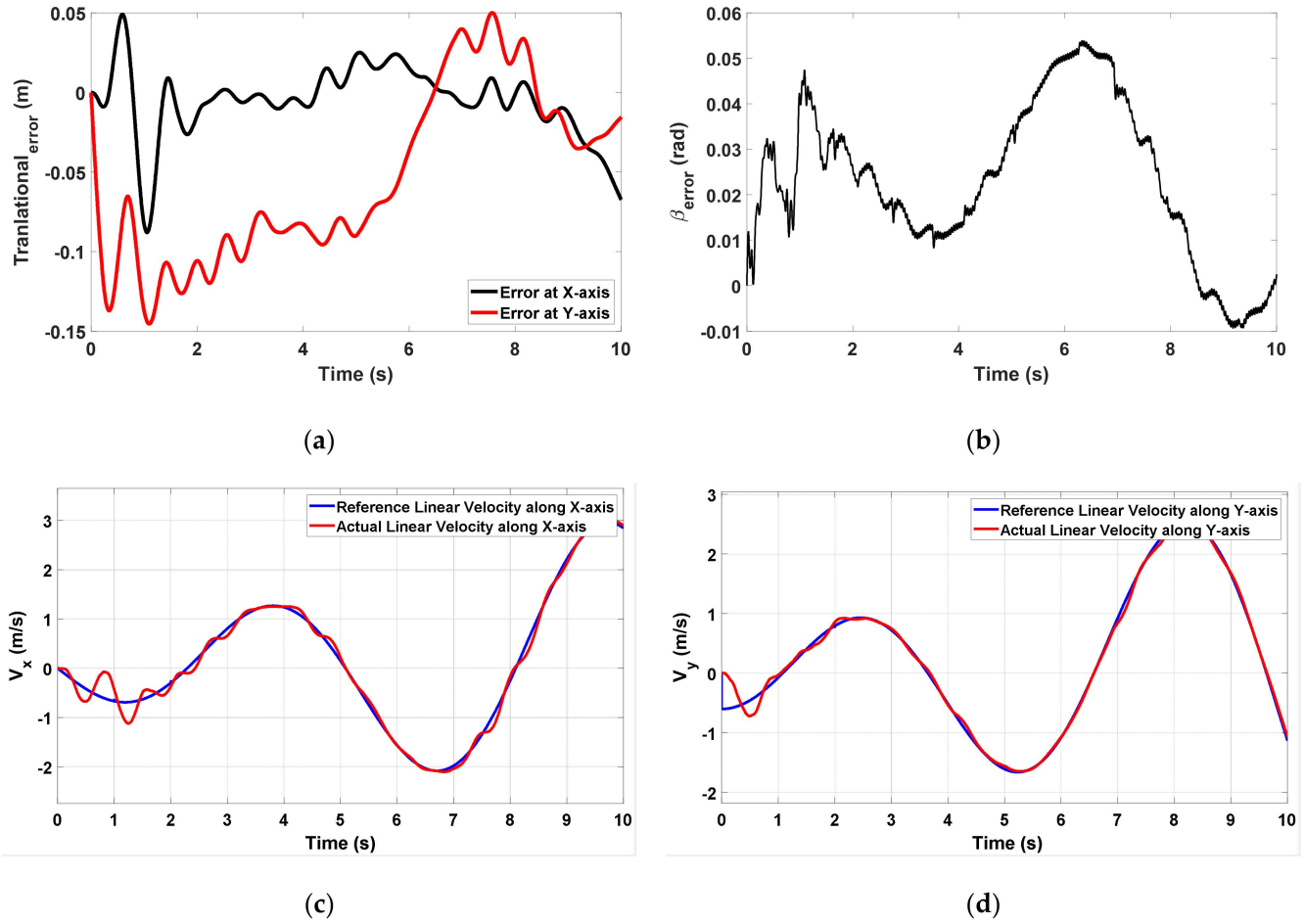

Figure 9. (**a**) The translational motion errors of the AGV at X and Y axis during the spiral path. (**b**) The rotational motion error of the AGV. (**c**) The reference and actual linear velocity of the AGV along X axis. (**d**) The reference and actual linear velocity of the AGV along Y axis.

In addition, the results in Figure 9b show the error in the rotational motion made by the AGV throughout the motion. According to these results, a maximum error of 0.06 rad was observed in the rotational motion along the entire route, and the average rotational error of the AGV is calculated to be 0.0228 rad. According to these results, it can be said that the AGV successfully follows the reference route both in translation and rotation with little error. These results can also be supported by linear velocities in the x and y directions. Figure 9c,d show the time variation of the instantaneous and reference linear velocities of the AGV in the x and y directions for the movement along the spiral route. As can be seen from the figures, errors are reduced in following the reference linear velocities calculated based on the reference orbit.

Another indicator of successful tracking performance and the power consumed while achieving this tracking performance is the angular rotational speed of the wheels. The angular rotational speeds of the wheels are obtained by feeding DC motors from DC/DC converters. These voltage values are determined by the optimal PID controllers calculated by Optimizer-1, which provides angular velocity-based route control, and are obtained from the outputs of DC/DC converters, similar to reference voltages as much as possible, in line with the optimal parameters determined by Optimizer-2.

For this reason, it is very important for low power consumption and successful path-tracking performance that the errors in the changes in the angular velocity of the wheels are low because these angular velocities sent to the wheels via the motors are determined by both optimizers on the basis of the lowest possible power consumption and maximum track performance. Figure 10 shows the reference angular velocities for all four Mecanum

wheels, the instantaneous angular velocities of the AGV wheels along the route and the errors between these two speeds. The results show that the actual angular velocities shown with the red line successfully follow the reference angular velocities shown with the blue line for all four wheels. The variable structure observed in the instantaneous angular velocities in the figures is due to the voltage values from the DC/DC converters and the generation of these instantaneous wheel speeds because DC/DC buck converters use switching while reducing the high voltage value from the fuel cell to the specified reference voltage value, and this switching is performed with the PWM signal with a switching frequency (f_s = 10,000 Hz). Therefore, the reference angular velocity values have a flatter variation as calculated with kinematic equations, while the actual velocity values have more noise-like additives. When the results are examined, it is observed that the errors in wheel angular velocities generally vary between +0.02 and −0.02 rad/s for each wheel. In addition, when the average angular velocity errors are calculated for each wheel during the movement, it is seen that the values of 2.6578×10^{-5}, 6.7423×10^{-5}, 6.9445×10^{-4} and 2.6578×10^{-5} rad/s are obtained for each wheel. These results show that the developed control strategies both improve route-tracking performance and reduce power consumption as much as possible, and this is successfully implemented by the entire system.

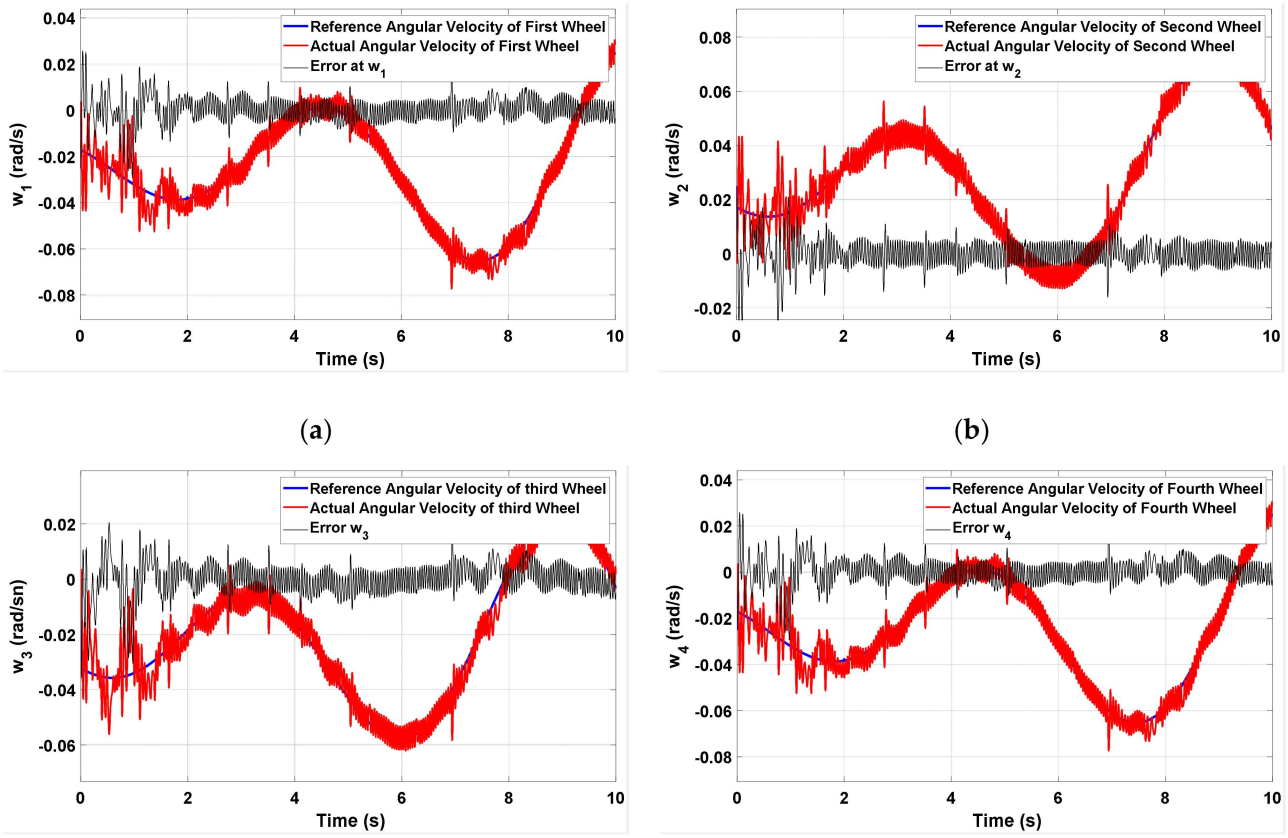

Figure 10. The comparison of reference and actual angular velocities (blue line: reference angular velocity, red line: actual angular velocity and black line: error between reference and actual velocity): (**a**) Mecanum wheel-1, (**b**) Mecanum wheel-2, (**c**) Mecanum wheel-3, (**d**) Mecanum wheel-4.

In the previous figure, the importance of the voltage-tracking performance of the DC/DC converter is mentioned. The reference voltages from the PID controllers that control the trajectory tracking are provided by DC/DC converters by reducing the high voltage from the fuel cell, which is the system supply. The voltage-tracking performance of these converters, the energy efficiency and tracking performance of which are adjusted

with the optimal parameters determined by Optimizer-2, is given in Figure 11 for the first and second motors. When the voltage-tracking performance given for the first motor in Figure 11a is examined, it is seen that a successful voltage tracking is obtained, and an error such as 0.3082 V appears as an average error. Similarly, in the voltage-tracking performance of the second DC/DC buck converter given in Figure 11b, the error between the reference control input voltage for the second motor and the voltage sent to the motor at the inverter output is calculated as 0.7385 V on average. For the third and fourth DC/DC converters, for which graphs of change over time are not given here, the errors between the reference and actual output voltages are calculated as 1.5624 and 0.6042 V, respectively. As seen in these error values, it was determined that the optimization-based controller designed for DC/DC converters provides a successful voltage-tracking performance. In addition, the aim was to minimize the power drawn from the fuel cell as much as possible in the design study and develop intelligent control strategies for DC/DC converters.

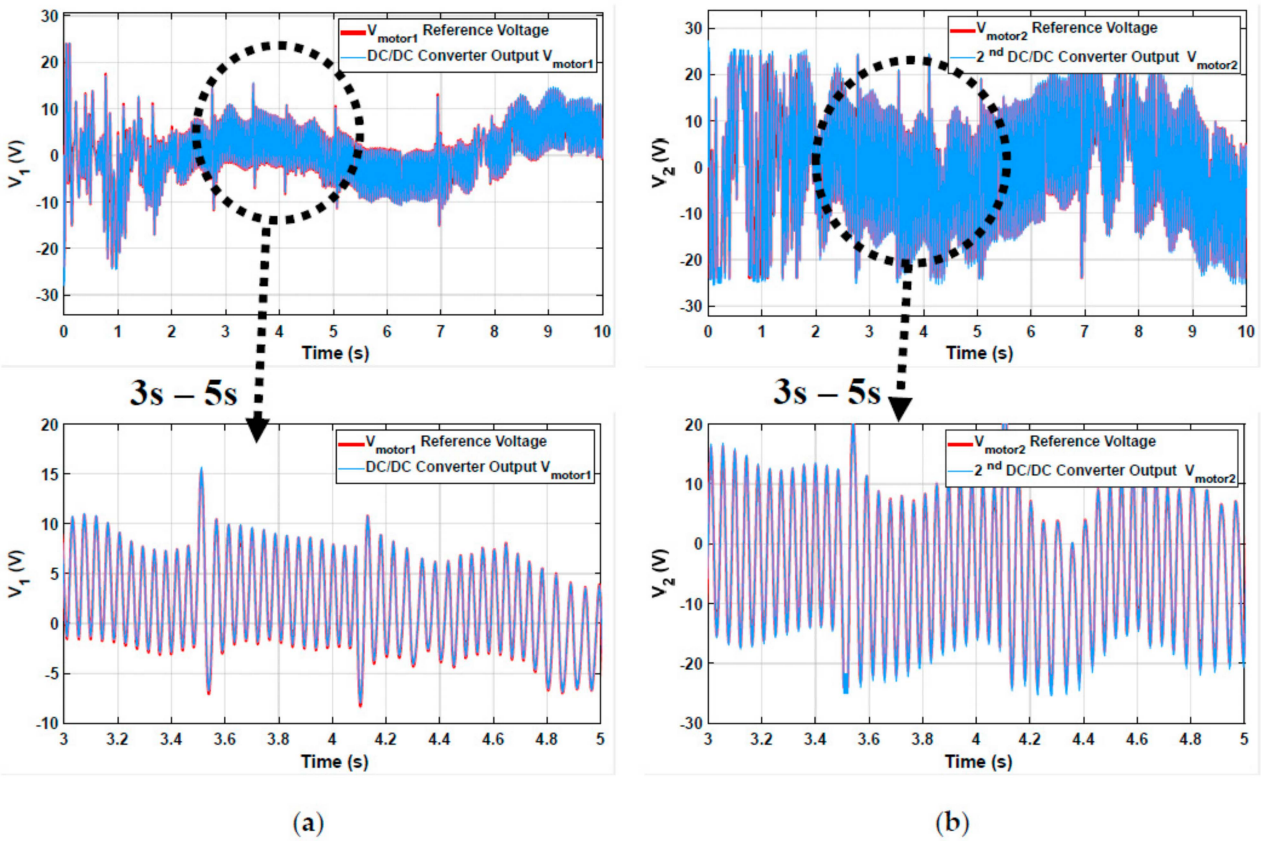

Figure 11. The comparison of the voltage-tracking performance of DC/DC converters (**a**) The reference and output voltage comparison for DC/DC converter 1. (**b**) The reference and output voltage comparison for DC/DC converter 2.

Minimization of power consumption has been included in the process based on the entire optimization algorithm and has been designed in terms of energy, cost and time savings as well as improved route-tracking performance. In this direction, the voltage and current fed to the system by the fuel cell were analyzed during the test for the spiral route. Figure 12a shows the variations of the fuel cell's supply voltage and consumed power as a function of the fuel cell's current. In accordance with the characteristics of the fuel cell, when the current drawn from the fuel cell increases, the supply voltage decreases, and the power drawn from the fuel cell increases. During the spiral routing motion, it is generally operated at lower currents depending on the choice of 24 V DC motors and AGV characteristics (weight, wheel, etc.). In addition, it is very important for energy efficiency to work at low current and low power in accordance with the goal of reducing power

consumption for all parameters determined by optimization algorithms. In Figure 12a, it is also observed that the data collected from the fuel cell are concentrated on the left side of the graph. According to the results obtained, the average voltage fed to the AGV system by the fuel cell throughout the process was calculated as 43.38 V. Similarly, the average current was observed as 1.4625 A. From the power–current graph, it can be seen that a maximum power consumption of 800 W is realized throughout the movement. The variation of power consumption according to the obtained optimal parameters of the AGV moving along the spiral route as a function of time is shown in Figure 12b. According to these results, the average power consumption on the fuel cell side during the movement is 58.2675 W. This shows that the design objectives of low power consumption and maximum tracking performance criteria were successfully met.

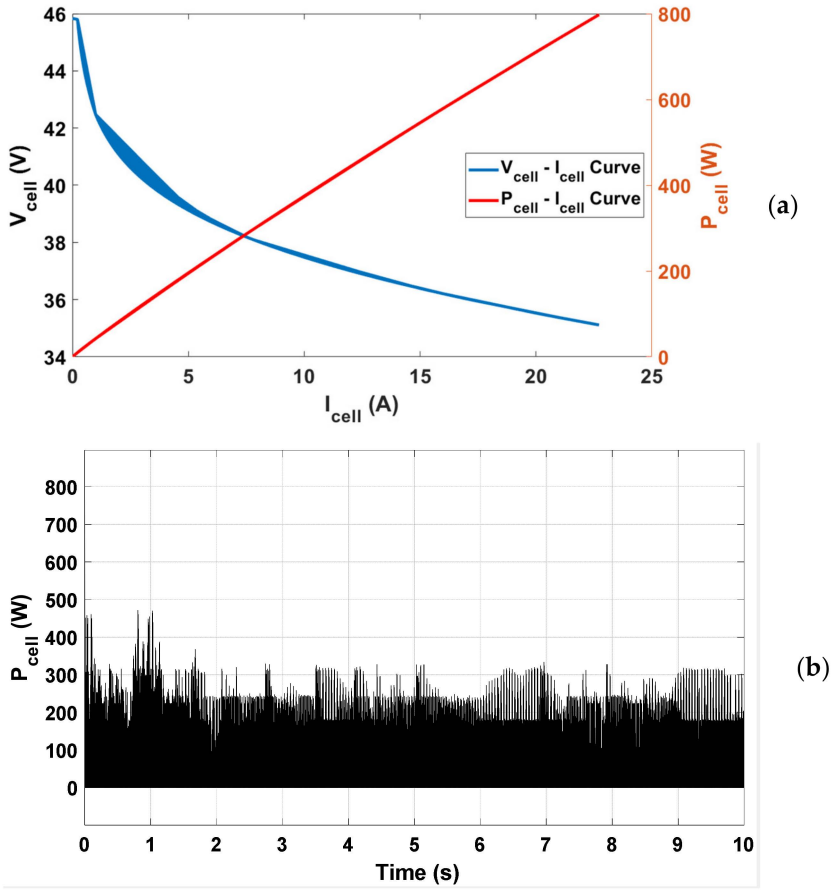

Figure 12. (**a**) The curves of $V_{cell} - I_{cell}$ and $P_{cell} - I_{cell}$ during the spiral route tracking of AGV. (**b**) The variation of the consumed power during the spiral route tracking of AGV.

In addition to all these analyses, the consumption of the fuel and air by the PEMFC during the movement was also examined. Figure 13a shows the variations in fuel and air consumption by the fuel cell as a function P_{cell} while following the spiral route. As seen in the figure, air consumption is higher than fuel consumption. It is seen that both fuel and air are consumed more at low power consumption. As stated in the previous figure, the data collected from the fuel cell generally show that a low amount of power is consumed during the movement, and accordingly, the optimization-based intelligent control strategies and the selection of the converter parts also cause low fuel consumption. Figure 13b shows the variations in fuel and air consumption by the fuel cell while following the spiral route. The results show that the average air and fuel consumption during the movement is 1.02 and 0.432 lpm, respectively.

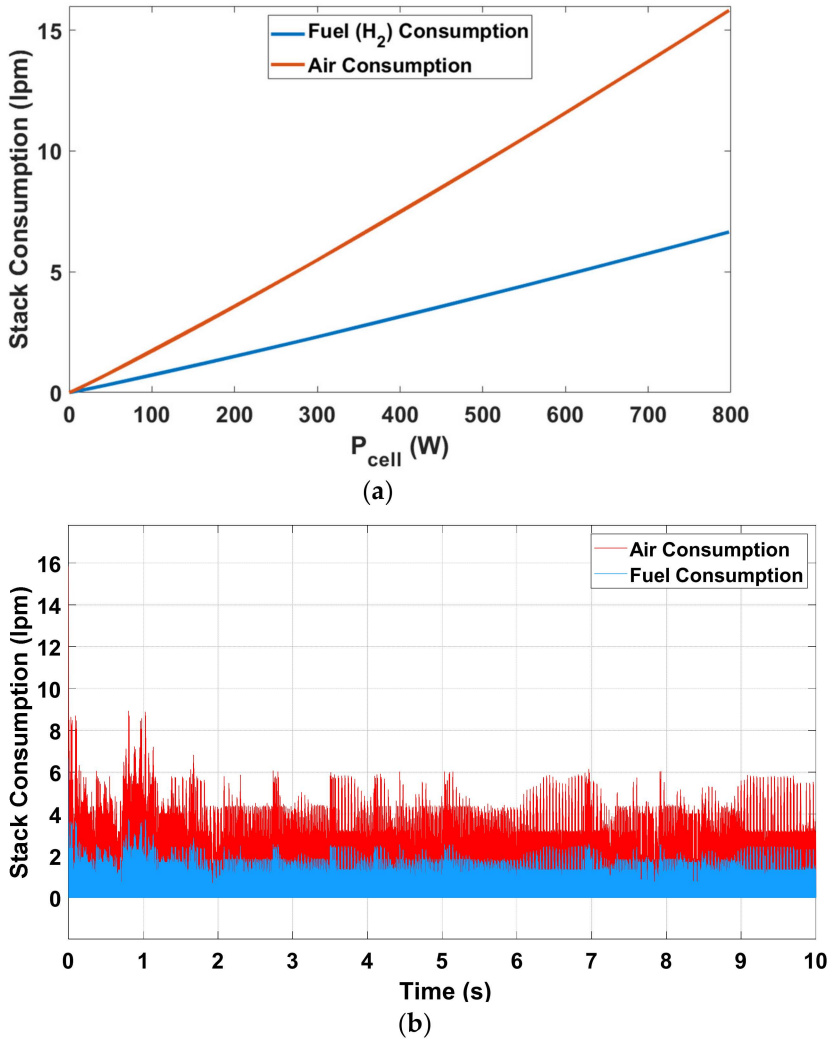

Figure 13. (**a**) The variation of the fuel and air consumption of the PEM fuel cell as a function of consumed power from the fuel cell during the spiral route tracking of AGV. (**b**) The variations in fuel and air consumption of the PEM fuel cell as a function of time.

5. Conclusions

The use of alternative energy sources in the industry has increased in recent years, and AGV systems used in industry are also becoming compatible with alternative energy sources due to their cost, environmental and time advantages. In this study, the optimized design and modeling and a development control strategy to ensure maximum route-tracking performance with reduced power consumption are emphasized for an AGV system with a PEMFC, which is an alternative energy source that supports the concept of energy independence. After modeling the full FCAGV system with its subsystem, such as DC/DC converters, motors, AGV and fuel cells, the PSO-based controllers and converters were designed, and optimal values of the coefficients of controllers and values of the components of each converters were determined in order to achieve more successful trajectory tracking performance with reduced power consumption. These optimal parameters were obtained by analyzing with different trajectories, and tests were conducted to analyze the performance of the AGV with these parameters. The results show that the AGV has successful path-tracking and lower power-consumption performance for the given reference spiral path. The observed path-tracking errors of FCAGV were less than 6 cm and 0.03 rad for all translational and rotational motions, respectively. These data show that the designed FCAGV system has sufficient path-tracking performance for both translational and rotational motions. The average voltage-tracking error for all converters

is approximately 0.75 V, and this shows that the DC/DC converters have successful and sufficient voltage-tracking performance with few errors. Power consumption is another important factor for the optimization process, and the average power consumption of the fuel cell is observed approximately 58.2675 W during 10-second movements. This shows the energy efficient performance of the designed FCAGV with the developed optimized control strategies. Based on these results, it is seen that the hydrogen-fueled AGV designed with the developed controllers is suitable for longer periods of operation with high energy efficiency and high route-tracking performance in areas such as factories and warehouses. In the future studies, these simulation results can be proved with experimental tests of the FCAGV system, and the different optimization algorithms can be used for the optimizers and comparison of the performance of these algorithms.

Author Contributions: Conceptualization, M.H.D.; methodology, M.H.D. and M.D.; software, M.H.D.; investigation, M.H.D. and M.D.; writing—original draft preparation, M.H.D. and M.D.; writing—review and editing, M.H.D.; visualization, M.H.D. and M.D.; supervision, M.H.D. All authors have read and agreed to the published version of the manuscript.

Funding: This research received no external funding.

Institutional Review Board Statement: Not applicable.

Informed Consent Statement: Not applicable.

Data Availability Statement: Data sharing not applicable.

Conflicts of Interest: The authors declare no conflict of interest.

References

1. Vis, I.F.A. Survey of research in the design and control of Automated Guided Vehicle Systems. *Eur. J. Oper. Res.* **2006**, *170*, 677–709. [CrossRef]
2. Haefner, L.E.; Bieschke, M.S. ITS opportunities in port operations. In Proceedings of the 1998 Transportation Conference Proceedings, Ames, IA, USA, 19 August 1998; pp. 131–134.
3. Kaloutsakis, G.; Tsourveloudis, N.; Spanoudakis, P. Design and development of an automated guided vehicle. In Proceedings of the IEEE International Conference on Industrial Technology, Maribor, Slovenia, 10–12 December 2003; Volume 2, pp. 990–993. [CrossRef]
4. Chen, Z.-Y.; Liaw, P.-R.; Nguyen, V.L.; Lin, P.T. Design of a high-payload mecanum-wheel ground vehicle (MWGV). *Robot. Syst. Appl.* **2021**, *1*, 24–34. [CrossRef]
5. Lin, X. Structural Design and Control Strategy of Magnetic Navigation AGV. *J. Jilin Inst. Chem. Technol.* **2019**, *7*, 30–35.
6. Doan, P.G. Automated Guided Vehicle (AGV) System. US Patent US8527153B2, 3 September 2013.
7. Pipes, G.R. Automated Guided Vehicle. US Patent US4657463A, 14 April 1987.
8. Cheong, H.-W.; Lee, H. Concept design of AGV (automated guided vehicle) based on image detection and positioning. *Procedia Comput. Sci.* **2018**, *139*, 104–107. [CrossRef]
9. González, D.; Romero, L.; del Mar Espinosa, M.; Domínguez, M. An optimization design proposal of automated guided vehicles for mixed type transportation in hospital environments. *PLoS ONE* **2017**, *12*, e0177944. [CrossRef]
10. Guo, J.; Liang, J. Design of AGV structure and Control System for hospital drug delivery. In *Advances in Mechanical Design*; Springer Nature: Singapore, 2022; pp. 1187–1202.
11. Zeidis, I.; Zimmermann, K. Dynamics of a four-wheeled mobile robot with Mecanum wheels. *ZAMM—J. Appl. Math. Mech./Z. Für Angew. Math. Und Mech.* **2019**, *99*, e201900173. [CrossRef]
12. Hendzel, Z.; Rykała, Ł. Modelling of dynamics of a wheeled mobile robot with Mecanum wheels with the use of Lagrange equations of the second kind. *Int. J. Appl. Mech. Eng.* **2017**, *22*, 81–99. [CrossRef]
13. Makatchev, M.; McPhee, J.J.; Tso, S.K.; Lang, S. System Design, Modelling, and Control of a Four-Wheel-Steering Mobile Robot. In Proceedings of the 19th Chinese Control Conference, Hong Kong, China, 6–8 December 2000; pp. 759–763.
14. Cherubini, A.; Passama, R.; Crosnier, A.; Lasnier, A.; Fraisse, P. Collaborative manufacturing with physical human–robot interaction. *Robot. Comput.-Integr. Manuf.* **2016**, *40*, 1–13. [CrossRef]
15. Saha, S.K.; Angeles, J. Kinematics and dynamics of a three-wheeled 2-DOF AGV. In Proceedings of the 1989 International Conference on Robotics and Automation, Scottsdale, AZ, USA, 14–19 May 1989; Volume 3, pp. 1572–1577. [CrossRef]
16. Stefek, A.; Pham, T.V.; Krivanek, V.; Pham, K.L. Energy comparison of controllers used for a differential drive wheeled mobile robot. *IEEE Access* **2020**, *8*, 170915–170927. [CrossRef]
17. Dhaouadi, R.; Hatab, A.A. Dynamic modelling of differential-drive mobile robots using Lagrange and Newton-Euler methodologies: A unified framework. *Adv. Robot. Autom.* **2013**, *2*, 1–7.

18. Xu, H.; Yu, Z.; Lu, X.; Wang, S.; Li, S.; Wang, S. Model predictive control-based path tracking control for automatic guided vehicles. In Proceedings of the 2020 4th CAA International Conference on Vehicular Control and Intelligence (CVCI), Hangzhou, China, 18–20 December 2020; pp. 627–632.
19. Han, Y.; Cheng, Y.; Xu, G. Trajectory tracking control of AGV based on sliding mode control with the improved reaching law. *IEEE Access* **2019**, *7*, 20748–20755. [CrossRef]
20. Chen, H. Terminal sliding mode tracking controller design for Automatic Guided Vehicle. *IOP Conf. Ser. Mater. Sci. Eng.* **2018**, *322*, 072035. [CrossRef]
21. Yu, R.; Zhao, H.; Zhen, S.; Huang, K.; Chen, X.; Sun, H.; Zhang, K. A novel trajectory tracking control of AGV based on Udwadia-Kalaba approach. *IEEE/CAA J. Autom. Sin.* **2017**, 1–13. [CrossRef]
22. Shi, S.; Yu, X.; Khoo, S. Robust finite-time tracking control of nonholonomic mobile robots without velocity measurements. *Int. J. Control* **2015**, *89*, 411–423. [CrossRef]
23. Zhang, K.; Sun, Q.; Shi, Y. Trajectory tracking control of autonomous ground vehicles using adaptive learning MPC. *IEEE Trans. Neural Netw. Learn. Syst.* **2021**, *32*, 5554–5564. [CrossRef] [PubMed]
24. Jacobs, L.; De Preter, A.; Anthonis, J.; Swevers, J.; Pipeleers, G. Trajectory tracking of agvs by linear parameter-varying control: A case study. *IFAC-PapersOnLine* **2018**, *51*, 43–48. [CrossRef]
25. Xu, H.; Zhu, J. Interval trajectory tracking for AGV based on MPC. In Proceedings of the 2019 Chinese Control Conference (CCC), Guangzhou, China, 27–30 July 2019; pp. 2835–2839. [CrossRef]
26. Bui, T.L.; Doan, P.T.; Kim, H.K.; Kim, S.B. Trajectory tracking controller design for AGV using laser sensor based Positioning System. In Proceedings of the 2013 9th Asian Control Conference (ASCC), Istanbul, Turkey, 26 June 2013; pp. 1–5. [CrossRef]
27. Wu, Y.; Wang, J.; Yin, X.; Zhao, H. Study for AGV trajectory control by using fuzzy reasoning. In Proceedings of the 2008 Fifth International Conference on Fuzzy Systems and Knowledge Discovery, Jinan, China, 18–20 October 2008; pp. 245–248. [CrossRef]
28. Setiawan, Y.D.; Nguyen, T.H.; Pratama, P.S.; Kim, H.K.; Kim, S.B. Path tracking controller design of four wheel independent steering automatic guided vehicle. *Int. J. Control Autom. Syst.* **2016**, *14*, 1550–1560. [CrossRef]
29. Hu, C.; Wang, R.; Yan, F.; Chen, N. Output constraint control on path following of four-wheel independently actuated autonomous ground vehicles. *IEEE Trans. Veh. Technol.* **2016**, *65*, 4033–4043. [CrossRef]
30. Sánchez-Ibáñez, J.R.; Pérez-del-Pulgar, C.J.; García-Cerezo, A. Path Planning for Autonomous Mobile Robots: A Review. *Sensors* **2021**, *21*, 7898. [CrossRef]
31. Dong, L.; Zichen, H.; Jiawei, W.; Chunwei, S. A review of mobile robot motion planning methods: From classical motion planning workflows to reinforcement learning-based architectures. *arXiv* **2021**, arXiv:2108.13619. [CrossRef]
32. Meißner, M.; Massalski, L. Modeling the electrical power and energy consumption of automated guided vehicles to improve the energy efficiency of production systems. *Int. J. Adv. Manuf. Technol.* **2020**, *110*, 481–498. [CrossRef]
33. Qiu, L.; Wang, J.; Chen, W.; Wang, H. Heterogenus AGV routing problem considering energy consumption. In Proceedings of the 2015 IEEE International Conference on Robotics and Biomimetics (ROBIO), Zhuhai, China, 6–9 December 2015; pp. 1894–1899. [CrossRef]
34. Kim, S.; Jin, H.; Seo, M.; Har, D. Optimal path planning of automated guided vehicle using dijkstra algorithm under dynamic conditions. In Proceedings of the 2019 7th International Conference on Robot Intelligence Technology and Application (RiTA), Daejeon, Republic of Korea, 1–3 November 2019; pp. 231–236. [CrossRef]
35. Riazi, S.; Bengtsson, K.; Lennartson, B. Energy optimization of large-scale AGV Systems. *IEEE Trans. Autom. Sci. Eng.* **2021**, *18*, 638–649. [CrossRef]
36. Kawakami, T.; Takata, S. Battery life cycle management for Automatic Guided Vehicle Systems. In *Design for Innovative Value Towards a Sustainable Society: Proceedings of EcoDesign 2011, Proceedings of the 7th International Symposium on Environmentally Conscious Design and Inverse Manufacturing, Kyoto, Japan, 30 November–2 December 2011*; Mitsutaka Matsumoto, M., Umeda, Y., Keijiro, M., Fukushige, S., Eds.; Springer: Dordrecht, The Netherlands, 2012; pp. 403–408.
37. Meziane, M.E.-A. Automated Guided Vehicles Battery Management for Industry 4.0. *J. Intell. Fuzzy Syst.* **2022**, *43*, 365–381. [CrossRef]
38. Şenaras, A.E.; Şenaras, O.M. Chapter 9: Battery Management of Automated Guided Vehicles Via System Dynamics. In *Internet of Energy Handbook*, 1st ed.; Kumar, P., Nikolovski, S., Dong, Z.Y., Eds.; CRC Press: Boca Raton, FL, USA, 2021. [CrossRef]
39. Zhan, X.; Xu, L.; Zhang, J.; Li, A. Study on agvs battery charging strategy for improving utilization. *Procedia CIRP* **2019**, *81*, 558–563. [CrossRef]
40. Kabir, Q.S.; Suzuki, Y. Increasing manufacturing flexibility through battery management of Automated Guided Vehicles. *Comput. Ind. Eng.* **2018**, *117*, 225–236. [CrossRef]
41. Kendall, K.; Liang, B.; Kendall, M. Microtubular SOFC (msofc) system in Mobile Robot Applications. *ECS Trans.* **2017**, *78*, 237–242. [CrossRef]
42. Guizzi, G.L.; Manno, M.; De Falco, M. Hybrid fuel cell-based energy system with metal hydride hydrogen storage for small mobile applications. *Int. J. Hydrogen Energy* **2009**, *34*, 3112–3124. [CrossRef]
43. Lü, X.; Chen, C.; Wang, P.; Meng, L. Status evaluation of mobile welding robot driven by fuel cell hybrid power system based on Cloud model. *Energy Convers. Manag.* **2019**, *198*, 111904. [CrossRef]
44. Niestrój, R.; Rogala, T.; Skarka, W. An energy consumption model for designing an AGV energy storage system with a PEMFC STACK. *Energies* **2020**, *13*, 3435. [CrossRef]

45. DC Motor Speed: System Modeling. Available online: https://ctms.engin.umich.edu/CTMS/index.php?example=MotorSpeed&section=SystemModeling (accessed on 18 February 2023).
46. Erickson, R.W.; Maksimovi'c, D. *Fundamentals of Power Electronics*, 2nd ed.; Kluwer Academic Publishers: Norwell, MA, USA, 2001.
47. Hella, M.M.; Mercier, P.P. *Power Management Integrated Circuits*, 1st ed.; CRC Press Publishers: Boca Raton, FL, USA, 2016.
48. Model PEM Fuel Cells with Simulink and Simscape. Available online: https://www.mathworks.com/discovery/fuel-cell-model.html (accessed on 18 February 2023).
49. Datta, A.; Ho, M.-T.; Bhattacharyya, S.P. *Structure and Synthesis of PID Controllers*; Springer: London, UK, 2010.
50. Ho, M.-T.; Lin, C.-Y. PID controller design for robust performance. In Proceedings of the 41st IEEE Conference on Decision and Control, Las Vegas, NV, USA, 10–13 December 2002.
51. Kim, T.-H.; Maruta, I.; Sugie, T. Robust PID controller tuning based on the constrained particle swarm optimization. *Automatica* **2008**, *44*, 1104–1110. [CrossRef]
52. Ou, C.; Lin, W. Comparison between PSO and GA for parameters optimization of Pid Controller. In Proceedings of the 2006 International Conference on Mechatronics and Automation, Luoyang, China, 25–28 June 2006.
53. Dutta, P.; Nayak, S.K. Grey Wolf optimizer based PID controller for Speed Control of BLDC Motor. *J. Electr. Eng. Amp Technol.* **2021**, *16*, 955–961. [CrossRef]
54. Abachizadeh, M.; Yazdi, M.R.; Yousefi-Koma, A. Optimal tuning of PID controllers using artificial bee colony algorithm. In Proceedings of the 2010 IEEE/ASME International Conference on Advanced Intelligent Mechatronics, Montreal, QC, Canada, 6–9 July 2010.
55. Kennedy, J.; Eberhart, R. Particle swarm optimization. In Proceedings of the ICNN'95—International Conference on Neural Networks, Perth, WA, Australia, 27 November–1 December 1995; Volume 4, pp. 1942–1948. [CrossRef]